Transmission of coherent phonons through a metallic multilayer

D. J. Dieleman, A. F. Koenderink, M. G. A. van Veghel, A. F. M. Arts, and H. W. de Wijn
Faculty of Physics and Astronomy, and Debye Institute, Utrecht University, P.O. Box 80.000, 3508 TA Utrecht, The Netherlands
(Received 2 January 2001; revised manuscript received 21 May 2001; published 5 October 2001)

The transmission of a coherent beam of longitudinal acoustic phonons through a 12-layer Ag-Au superlattice is measured with high resolution at gigahertz frequencies. The phonons are generated with laser-induced thermomodulation of a Au transducer and, after passage through the superlattice, detected with Brillouin scattering in the $PbMoO_4$ single-crystalline substrate. The transmission is found to drop to about 1% in well-defined stop bands. Calculations based on wave equations with inclusion of acoustic damping quantitatively reproduce the stop bands as well as the oscillatory frequency dependence of the transmission at intermediate frequencies.

DOI: 10.1103/PhysRevB.64.174304 PACS number(s): 63.20.−e

I. INTRODUCTION

Superlattices, periodic or quasiperiodic layered arrays, derive their interest primarily from the occurrence of frequency zones that are forbidden for the transmission of waves that are commensurate with the underlying periodicity. With regard to acoustic waves, in the course of the last two decades a number of experimental studies have been devoted to the observation of stop bands in strictly periodic superlattices[1–4] as well as quasiperiodic superlattices based on the Fibonacci sequence.[5,6] The experimental work has concentrated on superlattices made up of bilayers of crystalline or amorphous semiconductors, notably $GaAs/Al_xGa_{1-x}As$. Use was made of phonon transmission spectroscopy based on superconducting tunnel junctions,[1–3] which despite the limited resolution detected dips in the phonon transmission in specific frequency regions, and further frequency-selective phonon imaging[4,6] and Raman scattering.[5,7] Theoretical studies, which are not hindered by the limited frequency and angular resolution of common phonon sources and detectors, have addressed a great variety of systems, varying from periodic superlattices to randomly stacked multilayers.[8–10]

In the present paper, we investigate the transmission of acoustic waves through a periodic superlattice at gigahertz frequencies. As distinct from previous studies, the superlattice is metallic and the acoustic wave is to a high degree coherent and directional. The unparalleled resolution offered by the use of coherent phonons allows us to measure the transmission to such detail that we observe a drop by two orders of magnitude in the first two stop bands, an oscillatory frequency dependence in the passbands because of the finite number of layers, and a narrow ''impurity'' mode associated with the phonon-generating transducer. Calculations based on wave equations faithfully reproduce these features. Agreement with theory is, however, not achieved without account for frequency-dependent acoustic damping.

II. EXPERIMENTS

A coherent Fresnel-diffracted acoustic wave, tunable in frequency, is generated by the use of cw laser-induced thermomodulation of a thin metallic transducer.[11] The wave, longitudinally polarized, approximately 40 μm in diameter and of typically 1-MHz spectral purity, passes through the superlattice and travels onward into a single crystal of lead molybdate ($PbMoO_4$), where, after a short distance of travel (≈ 0.1 mm), it is frequency, wave vector, and site selectively detected with Brillouin scattering. $PbMoO_4$ was chosen for its high Brillouin-scattering efficiency and optical transparency. For further details of the experimental procedures and setup, reference is made to Ref. 12.

The crystal is a cuboid measuring $10\times10\times5$ mm^3 with the c axis parallel to the larger sides. A periodic superlattice consisting of 12 alternate Au and Ag layers was deposited by physical vapor deposition onto half of a (001) face. Next, the whole (001) face was covered with a Au layer serving as transducer. Intermediate layers of Cr, thin enough (≈ 5 nm) to be acoustically insignificant, improved the superlattice-crystal and transducer-superlattice adhesion. The deposition was monitored *in situ* to ensure less than 0.3% variations in the layer thicknesses. The thickness of the superlattice as well as the total thickness of Ag deposited were determined absolutely after completion of the deposition, to find $d_{Au}=669$ nm and $d_{Ag}=334$ nm for the individual layers.

The thickness d_0 of the transducer derives from the acoustic intensity Φ_0 injected into the crystal by the bare transducer, which exhibits maxima at multiples of 1.50 ± 0.04 GHz as a result of double-fixed-end resonances.[12] Comparison with the theoretical Φ_0 (cf. the case $N=0$ in Fig. 3 below) yields $d_0=1080\pm30$ nm.

Partial coverage of a crystal face with the superlattice allows us to measure the acoustic intensity Φ_N after passage through the superlattice with reference to the intensity Φ_0 injected by the bare transducer. Taking the ratio Φ_N/Φ_0 eliminates the Brillouin cross section, the effects of acoustic attenuation in the $PbMoO_4$ substrate,[12] and the uncertainties associated with realignment of the Brillouin spectrometer from one frequency to the next. To integrate the Brillouin intensities over the acoustic beam as necessary for an accurate determination of Φ_N and Φ_0, we scanned perpendicularly to the pencil-shaped detection volume in 5-μm steps and fitted Gaussians to the acoustic profiles so measured.

In Fig. 1, Φ_N/Φ_0 is displayed for frequencies ranging from 1.5 to 5.8 GHz and seen to drop to order 1% in stop

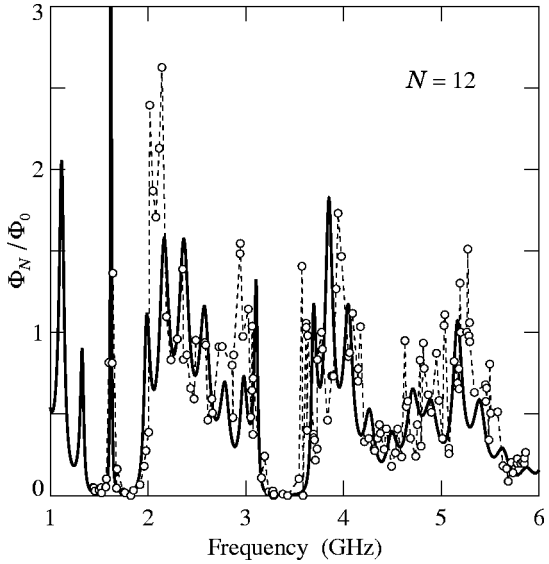

FIG. 1. The frequency dependence of the acoustic transmission through a 12-layer Au-Ag superlattice positioned between a Au transducer and a $PbMoO_4$ crystal. The ratio Φ_N/Φ_0 is the acoustic intensity measured below the superlattice with reference to the intensity below the bare transducer. The data points are connected by a dashed line for clarity. Stop bands are observed around 1.7 and 3.3 GHz. The narrow peak in the first stop band stems from a high-gain standing wave between the front end of the transducer and the superlattice-crystal interface. The solid curve represents Φ_N/Φ_0 calculated in Sec. III, but with inclusion of damping.

bands located in the frequency intervals 1.4–1.9 and 3.2–3.6 GHz, except for a high-gain resonance at 1.64 GHz. The data in Fig. 1 exhibit oscillations between the stop bands. To verify that these are real, supplementary measurements of Φ_N/Φ_0 were performed without realignment of the Brillouin spectrometer over frequency intervals as wide as permitted with a somewhat relaxed Brillouin condition (typically 0.4 GHz). We note in this context that the Brillouin cross section is frequency independent for longitudinal phonons and light polarized perpendicularly to the scattering plane.[13]

III. ACOUSTIC FLUX VERSUS FREQUENCY

To derive the acoustic intensity in the crystal, we solve the coupled wave equations for the atomic displacements $u(z,t)$ in transducer, superlattice, and crystal. The force driving the waves is the oscillatory temperature distribution within the transducer,[12]

$$\vartheta(z,t)=\frac{\Phi_{\rm opt}}{\sqrt{\omega K C_V}}e^{-\alpha z}\cos\left(\alpha z-\omega t-\frac{1}{4}\pi\right), \qquad (1)$$

which results from diffusive transport of the oscillatory heat flux $\Phi_{\rm opt}\sin\omega t$ deposited onto the outer surface of the transducer by the interfering lasers. Here, ω is the angular frequency, C_V is the specific heat, and K the thermal conductivity (Table I). Equation (1) holds as long as the transducer thickness amply exceeds the thermal skin depth $\alpha^{-1}=(2K/\omega C_V)^{1/2}$, which amounts to 200 nm at 1 GHz. The finite extent of the thermal strain source and the strong coupling between transducer and superlattice necessitate us to consider the wave equations and their solutions in some detail.

TABLE I. Material properties of gold and silver.[a]

Property	Au	Ag	Units
ρ	19.3	10.5	10^3 kg/m^3
v[b]	3.24	3.65	10^3 m/s
C_V	2.49	2.52	10^6 J/m^{3}K
K	3.18	4.29	10^2 W/m K
β	14.0	19.2	10^{-6} K^{-1}
E_T	78.0	82.7	10^9 Pa
η	0.44	0.37	

[a]Reference 23.
[b]Longitudinal velocity $\|c$ axis.

If β_0 denotes the linear thermal expansion coefficient, $\vartheta(z,t)$ induces a strain of size $\beta_0\vartheta(z,t)$ counteracting the elastic strain $\varepsilon(z,t)=\partial u(z,t)/\partial z$. The total stress thus amounts to $\sigma(z,t)=C[\varepsilon(z,t)-\beta_0\vartheta(z,t)]$,[14] and beyond the transducer $\sigma(z,t)=C\varepsilon(z,t)$, with C the appropriate elastic constant. When indexing variables, material properties, and distances by $n=0$ through $N+1$ as defined in Fig. 2, the wave equations to be solved read

$$\frac{\partial^2 u_0}{\partial z^2}-\frac{1}{v_0^2}\frac{\partial^2 u_0}{\partial t^2}=\beta_0\frac{\partial\vartheta(z,t)}{\partial z} \quad (z\leqslant d_0), \qquad (2)$$

$$\frac{\partial^2 u_n}{\partial z^2}-\frac{1}{v_n^2}\frac{\partial^2 u_n}{\partial t^2}=0 \quad (n\geqslant 1;\ d_{n-1}\leqslant z\leqslant d_n), \qquad (3)$$

in which v_n denotes the longitudinal sound velocity. All waves are perpendicular to the transducer and multilayer.

In the various layers as well as the transducer, both forward and backward running waves build up as a result of multiple reflection. The wave launched into the crystal, on the other hand, never returns. The solution of Eqs. (2) and (3) with Eq. (1) substituted accordingly takes on the form

$$u_0(z)=a_0e^{iq_0z}+a_0'e^{-iq_0z}+\frac{2i\alpha\beta_0\Phi_{\rm opt}}{\sqrt{\omega K C_V}(q_0^2-2i\alpha^2)}e^{(i-1)\alpha z}, \qquad (4)$$

$$u_n(z)=a_ne^{iq_nz}+a_n'e^{-iq_nz} \quad (1\leqslant n\leqslant N), \qquad (5)$$

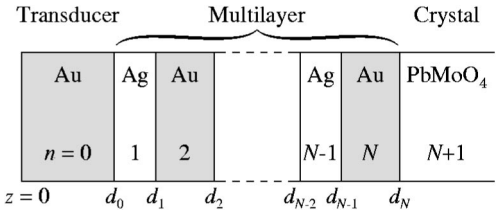

FIG. 2. Schematic representation of the transducer, superlattice, and crystal.

$$u_{N+1}(z) = a_{N+1} e^{iq_{N+1}z}, \tag{6}$$

in which $q_n = \omega/v_n$ are the wave vectors, a_n and a_n' denote the amplitudes, and the common time dependence $e^{-i\omega t}$ has been omitted. As for the boundary conditions, the stress must balance out at the outer surface, i.e., $\partial u_0(0)/\partial z = \beta_0 \vartheta(0,t)$, while displacement and stress are continuous across the interfaces.

The propagation of the acoustic wave through the superlattice itself is conveniently treated by the use of 2×2 layer-specific transfer matrices connecting the ends of the individual layers, such as previously applied to optical[15,16] and acoustic[8,17,18] multilayers. Equation (5) is accordingly implemented by

$$\begin{pmatrix} u_n \\ \sigma_n \end{pmatrix}_{d_n} = T_n \begin{pmatrix} u_n \\ \sigma_n \end{pmatrix}_{d_{n-1}}, \tag{7}$$

$$T_n = \begin{pmatrix} \cos\delta_n & (C_n q_n)^{-1} \sin\delta_n \\ -C_n q_n \sin\delta_n & \cos\delta_n \end{pmatrix}, \tag{8}$$

with $\delta_n = q_n(d_n - d_{n-1})$ the acoustic thickness. We have $C_n = \rho_n v_n^2$, in which ρ_n is the mass density.

Summing up, we are left with numerically solving the inhomogeneous linear equations (4) and (6) for a_0, a_0', and a_{N+1} under the constraint of the outer boundary condition, while $T_{\rm SL} = \Pi_{n=1}^{N} T_n$ connects u_{N+1} at $z = d_N$ with u_0 at $z = d_0$. The acoustic flux Φ_N inside the crystal, i.e., the quantity measured by Brillouin scattering, can subsequently be calculated from

$$\Phi_N = \tfrac{1}{2} \rho_{N+1} v_{N+1}^3 |\varepsilon_{33}|^2, \tag{9}$$

in which $|\varepsilon_{33}| = q_{N+1} a_{N+1}$ is the strain amplitude.

IV. DISCUSSION

Figure 3 displays the calculated acoustic energy flux Φ_N transmitted through the coupled system of transducer and superlattice in the frequency interval of interest, with $\Phi_{\rm opt}$ set to the typical value 10^8 W/m^2. The case $N=12$ in Fig. 3 pertains to the experiment. For comparison, Fig. 3 also shows the results, based on the same individual layer thicknesses, for multilayers that are half ($N=6$) and twice ($N=24$) as thick. Figure 3 also includes the result for the bare transducer ($N=0$), computed after setting $T_{\rm SL}$ equal to the unit matrix, which duplicates the corresponding analytical solution derived in Ref. 12.

In Eqs. (2) and (3) the acoustic wave is assumed to propagate through the transducer and superlattice without loss. In particular at the higher frequencies, however, acoustic damping reduces the transmitted flux. It further weakens the resonances in the frequency spectrum by diminishing the range over which the waves interfere. Acoustic damping can be incorporated by substituting $q_n + i\gamma$ for q_n everywhere in Eqs. (4)–(6), with γ the reciprocal amplitude attenuation length. No frequency-specific data are available for acoustic attenuation in Au and Ag in the gigahertz range. For an estimate, we therefore consider three possible mechanisms:

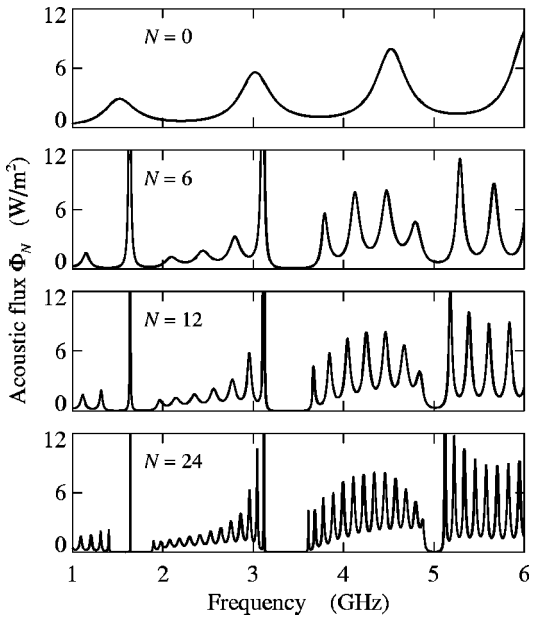

FIG. 3. The evolution with N of the theoretical acoustic energy flux Φ_N transmitted through a superlattice consisting of N alternating Ag and Au layers sandwiched between a Au transducer and a crystal of $PbMoO_4$. The case $N=12$, yet with damping, refers to the experiment in Fig. 1.

electron-phonon interaction, mass-defect scattering, and the thermoelastic effect. Relaxation of phonons by interaction with conduction electrons has been considered by Pippard,[19] who derived theoretical expressions applicable to simple metals. Inserting the electron mean free path $l \sim 4\times 10^{-8}$ m derived from the resistivity, we find negligible damping of longitudinal phonons in the relevant frequency range ($\gamma^{-1} \gtrsim 1$ mm for both Au and Ag). Note that at room temperature l is short enough for the hydrodynamic regime ($ql \ll 1$) to apply. Mass-defect scattering by isotopes and impurities, which scales with ω^4,[20] has even longer mean free paths at our frequencies. The thermoelastic effect, on the other hand, has found experimental confirmation in Zn for longitudinal waves up to 150 MHz.[21] In a phenomenological treatment,[22] the attenuation constant against thermoelastic damping at temperature T is given by

$$\gamma = \frac{1}{2v\tau_c} \frac{1+\eta}{(1-2\eta)(1-\eta)} \frac{\beta^2 T E_T}{C_V} \frac{\omega^2\tau_c^2}{1+\omega^2\tau_c^2}, \tag{10}$$

in which $\tau_c = K/C_V v^2$ is the characteristic time for thermal conduction, E_T is Young's modulus for isothermal deformation, and η is Poison's ratio (Table I). At 5.5 GHz, $\gamma^{-1} = 13$ μm for Au and 19 μm for Ag, compared to the 6.0-μm thickness of the superlattice.

For $N=12$, the theoretical ratio Φ_N/Φ_0 with inclusion of thermoelastic damping is compared with experiment in Fig. 1, where it has been inserted as the solid curve. In view of the absence of fitting parameters, theory is found to agree remarkably well with experiment. The most salient stop band extends over the interval 3.2–3.6 GHz. At its middle frequency, 3.36 GHz, a full acoustic wavelength precisely

equals the thickness of a single Au-Ag bilayer, i.e., $\omega(d_{\mathrm{Au}}/v_{\mathrm{Au}}+d_{\mathrm{Ag}}/v_{\mathrm{Ag}})=2\pi$. If suppression of the transmission is a measure for the quality of the stop band, in the experiment Φ_N/Φ_0 drops to 6×10^{-3} at the lowest point, compared to $\Phi_N/\Phi_0=4\times10^{-3}$ from theory.

Equally well developed is a stop band around the middle frequency 1.68 GHz, for which half the acoustic wavelength matches a Au-Ag bilayer. It extends over an even wider range 1.4–1.9 GHz and has a similar suppression. The intimate coupling between multilayer and transducer, however, shows up in a narrow ''impurity'' mode at 1.64 GHz, reaching a peak as high as $\Phi_N/\Phi_0\sim10$. Nonetheless, this mode manifests the very nature of a stop band, namely, complete return of the incoming wave when it is commensurate with the superlattice. In the present case, the returning wave resonates with the lowest transducer mode, which lies near the center of the stop band (cf. Fig. 3), to form a standing wave spanning the combined length of transducer and superlattice. Its frequency is accordingly given by $\omega[(d_0+6d_{\mathrm{Au}})/v_{\mathrm{Au}}+6d_{\mathrm{Ag}}/v_{\mathrm{Ag}})]=7\pi$, as observed. The third stop band in the frequency range investigated, occurring around 5.0 GHz, is only marginally seen. Its width is smaller and its depth less pronounced, in keeping with the smallness of the Fourier component of the superlattice at that frequency. We finally point out that the number of transmission minima between stop bands should equal $\frac{1}{2}N$ (cf. Fig. 3). Also this feature is to a great extent recovered in the data, in particular between the first two stop bands.

V. CONCLUSIONS

In summary, we have measured the transmission of a coherent acoustic wave through a metallic Ag-Au superlattice at gigahertz frequencies with high resolution. The stop bands appear to extend over a substantial width and to suppress the transmission to order 1% or less, while in the frequency regimes between the stop bands oscillations in the transmission occur. Transfer matrices, yet with due account of acoustic damping as well as coupling with the phonon-generating transducer, provide an adequate quantitative description.

ACKNOWLEDGMENTS

The work was supported by the Netherlands Foundation ''Fundamenteel Onderzoek der Materie (FOM)'' and the ''Nederlandse Organisatie voor Wetenschappelijk Onderzoek (NWO).''

[1] V. Narayanamurti, H. L. Störmer, M. A. Chin, A. C. Gossard, and W. Wiegmann, Phys. Rev. Lett. **43**, 2012 (1979).
[2] O. Koblinger, J. Mebert, E. Dittrich, S. Döttinger, W. Eisenmenger, P. V. Santos, and L. Ley, Phys. Rev. B **35**, 9372 (1987).
[3] P. V. Santos, L. Ley, J. Mebert, and O. Koblinger, Phys. Rev. B **36**, 1306 (1987).
[4] D. C. Hurley, S. Tamura, and J. P. Wolfe, Phys. Rev. Lett. **58**, 2446 (1987); S. Tamura, D. C. Hurley, and J. P. Wolfe, Phys. Rev. B **38**, 1427 (1988).
[5] R. Merlin, K. Bajema, R. Clarke, F. Y. Juang, and P. K. Bhattacharya, Phys. Rev. Lett. **55**, 1768 (1985).
[6] D. C. Hurley, S. Tamura, J. P. Wolfe, K. Ploog, and J. Nagle, Phys. Rev. B **37**, 8829 (1988).
[7] D. J. Lockwood, R. L. S. Devine, A. Rodriguez, J. Mendialdua, B. Djafari Rouhani, and L. Dobrzynski, Phys. Rev. B **47**, 13 553 (1993).
[8] R. E. Camley, B. Djafari-Rouhani, L. Dobrzynski, and A. A. Maradudin, Phys. Rev. B **27**, 7318 (1983).
[9] M. J. Kelly, J. Phys. C **18**, 5963 (1985).
[10] S. Tamura and J. P. Wolfe, Phys. Rev. B **35**, 2528 (1987); **36**, 3491 (1987); **38**, 5610 (1988); S. Tamura and F. Nori, *ibid.* **40**, 9790 (1989); **41**, 7941 (1990); S. Mizuno and S. Tamura, *ibid.* **45**, 734 (1992).
[11] E. P. N. Damen, A. F. M. Arts, and H. W. de Wijn, Phys. Rev. Lett. **74**, 4249 (1995).
[12] E. P. N. Damen, D. J. Dieleman, A. F. M. Arts, and H. W. de Wijn, preceding paper, Phys. Rev. B **64**, 174303 (2001).
[13] J. R. Sandercock, in *Light Scattering in Solids III*, Topics in Applied Physics, Vol. 51, edited by M. Cardona and G. Güntherodt (Springer-Verlag, Berlin, 1982), p. 173.
[14] C. Thomsen, H. T. Grahn, H. J. Maris, and J. Tauc, Phys. Rev. B **34**, 4129 (1986).
[15] M. Born and E. Wolf, *Principles of Optics*, 6th ed. (Cambridge University Press, Oxford, 1997).
[16] M. Kohmoto, B. Sutherland, and K. Iguchi, Phys. Rev. Lett. **58**, 2436 (1987).
[17] M. Babiker, D. R. Tilley, E. L. Albuquerque, and C. E. T. Gonçalves da Silva, J. Phys. C **18**, 1269 (1985).
[18] H. T. Grahn, H. J. Maris, J. Tauc, and B. Abeles, Phys. Rev. B **38**, 6066 (1988).
[19] A. B. Pippard, Rep. Prog. Phys. **23**, 176 (1960); see also F. S. Kahn and P. B. Allen, Phys. Rev. B **35**, 1002 (1987).
[20] P. G. Klemens, Proc. R. Soc. London, Ser. A **68**, 1113 (1955).
[21] K. Lücke, J. Appl. Phys. **27**, 1433 (1956).
[22] R. Truell, C. Elbaum, and B. B. Chick, *Ultrasonic Methods in Solid State Physics* (Academic Press, New York, 1969), p. 180.
[23] Y. A. Touloukian *et al.*, *Thermophysical Properties of Matter* (IFI/Plenum, New York, 1970), Vols. 1, 4, 10, and 12.